Chemical Methodologies 5(2021) 271-284

Chemical Methodologies

Journal homepage: http://chemmethod.com

Original Research Article

Removal of Lead from Wastewater by Iron–Benzenetricarboxylate Metal-Organic Frameworks

Gholamreza Nabi Bidhendi[1], Naser Mehrdadi[1], Mehran Firouzbakhsh[2,*]

[1]*Department of Environmental Engineering, University of Tehran, Tehran, Iran*
[2]*PhD Student of Environmental Engineering, Water and Waste Water, University of Tehran, Kish International Campus, Kish, Iran*

ARTICLE INFO

Article history

Submitted: 2021-03-16
Revised: 2021-04-03
Accepted: 2021-05-05
Manuscript ID: CHEMM-2104-1326
Checked for Plagiarism: **Yes**
Language Editor:
Dr. Behrouz Jamalvandi
Editor who approved publication:
Dr. Metin Hayri Acar

DOI: 10.22034/chemm.2021.130208

KEYWORDS

Lead, Trimesic acid
Metal organic framework
Wastewater treatment

ABSTRACT

Iron–benzenetricarboxylate metal-organic frameworks were prepared chemically in the present study. For this purpose, using iron (II, III) chloride and trimesic acid, the nano metal-organic ramework was synthesized and then was identified and characterized by scanning tunneling electron microscopy, X-ray diffraction analysis, Fourier transform infrared spectrogram, ultraviolet, and N_2 adsorption and desorption (Brunauer-Emmett-Teller and Barrett- Joyner-Halenda) techniques. The structure, morphology, purity, and crystallinity of the metal-organic framework were also investigated. The framework was employed to remove lead from wastewater and the effect of different parameters, including absorbent concentration (0.2-0.5 mg/L), pH (3.5-12.5), temperature (10-75 °C), and lead concentration (10-150 mg/L), on lead removal was investigated. The maximum efficiency, as 100% lead removal, was obtained with 0.25 mg/L of BTC-Fe adsorbent at 50 °C and a pH of 3.4. Due to the features of the employed adsorbent, such as magnetic effects, reusability, large surface area, low cost, and high efficiency, it can be suggested as an ideal option for the removal of lead.

GRAPHICAL ABSTRACT

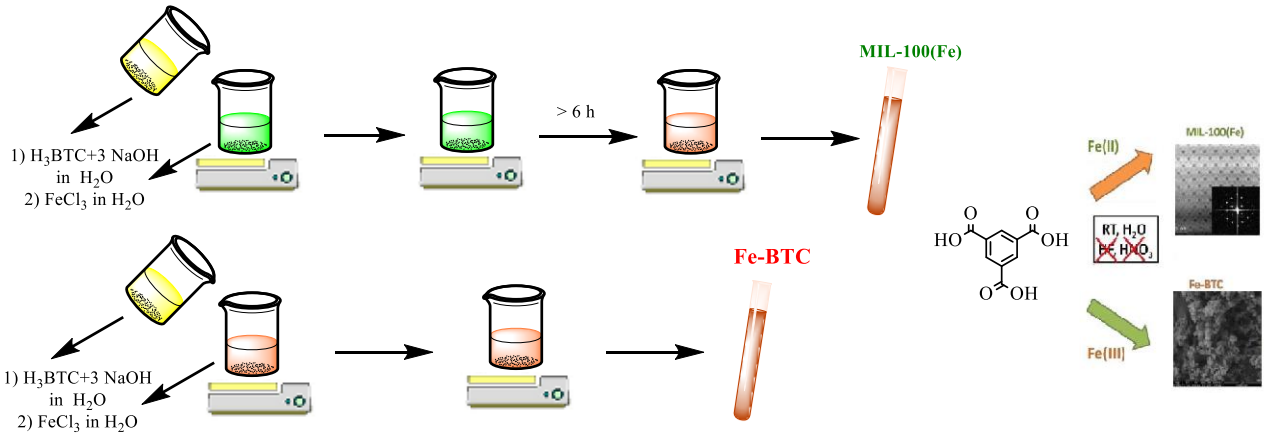

* Corresponding author: Mehran Firouzbakhsh
✉ E-mail: firouzbakhsh.meh@ut.ac.ir

Introduction

The entry of effluents containing lead into freshwater is a threat to the environment, and accordingly, the removal of heavy metals from industrial wastewater is of great importance [1]. Numerous methods, such as chemical deposition and membrane processes, as well as electrochemical, evaporation, minerals, etc., are utilized in the removal and separation of heavy metal ions from aqueous solutions; all have disadvantages, such as high cost of chemicals and equipment, the impossibility of recycling the adsorbent and adsorbate, and low efficiency. Adsorption processes are one of the effective methods in the removal of lead. Among the adsorbents, mesoporous silica and MCM molecular sieves, due to the high surface area, high porosity, spatial heterogeneity of pore-size distribution, and controllable surface area, are considered. These features make such materials a good choice for the adsorbent. Changes can be made to the channel walls or bound of different groups to their surfaces for increasing and improving these features. Besides, high efficiency, nanostructured adsorbents, with a large specific surface area and higher adsorption potential, produce less waste and are recoverable and reusable, which reduce cost and make the process cost-effective [2]. Shahbazi et al., in a recent study, used magnetic iron nanoparticles for the removal of lead and its recycling [3]. Alizadeh et al., investigated the synthesis of 2-mercaptobenzothiazole functionalized magnetic Fe to remove heavy metals, such as lead [4]. Despite many advantages, none of these methods had a maximum efficiency in the removal of heavy metals, such as lead [5]. Metal-organic frameworks, as a new class of advanced porous materials, have wide applications in the processes of adsorption and separation of heavy metals. They are coordination polymer compounds using a metal as a node and organic ligands as a binder. The size and shape of cavities in these crystalline and porous compounds can be engineered. These frameworks can be synthesized by binding metal clusters, as coordination centers, to organic ligands, as binders of mineral metal ions with specific physical and chemical properties. The first metal-organic framework, called five, was introduced (1999) and synthesized (2001) by Yaghi et al [6]. They synthesized it by the solvent, thermal method using zinc as a metal, carboxylic acid as a binder, and dimethylformamide as a solvent. This compound decomposes at above 350-400 °C, indicating its high thermal stability. Metal-organic frameworks also have high selectivity, poor guest-host interaction (desorption at lower temperatures), and high chemical stability. The 1,3,5-benzenetricarboxylate is an organic ligand, which its structure is shown in Figure 1 [7].

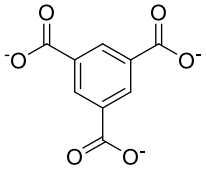

Figure 1: Chemical structure of trimesic acid ($C_9H_6O_6$) BTC^{3-}

In the present study, due to the low toxicity and high biocompatibility of iron, lead adsorption was performed using self-assembled iron metal-organic frameworks. Fe-BTC, a semi-amorphous non-crystalline material with photocatalytic properties, is the first synthesized framework, in which the effects of ultrasonic temperature (50 and 70 °C) and irradiation time (90 and 120 minutes) were investigated on its synthesis. It is synthesized similar to iron (III). The synthesized Fe-BTC nanoparticles show good photodissociation dynamics, and its 70 and 120 specimens have the highest photocatalytic activity. The second framework (MIL-100 (Fe)) is an octahedral zeolite equivalent to iron trimesate. Observations indicated that the catalytic activity of Fe-BTC is significantly higher [8].

Material and methods

Materials

The chemicals used in the present study included:

$FeCl_24H_2O$, $FeCl_36H_2O$, Pb $(NO_3)_2$, NH_4OH, HNO_3, HCl, C_2H_5OH, $Cu_3(BTC)_2$, and pH regulators, including NaOH, HCl, and H_3BTC (trimesic acid)

Equipment

Magnetic stirrer (IKA RH basic2), vibration magnetometer (Egg Princeton Applied VSM), atomic absorption spectrometer (Perkin-Elmer), scanning electron microscopy (CambridgeS-360), thermogravimetric analyzer under N_2 atmosphere (Meter), Fourier-transform infrared spectroscopy (FTIR), ultraviolet-visible spectroscopy (UV-Vis), ultrasonic bath, vacuum oven, a micro-analytical balance with 0.1 g accuracy, XRD device (Philips X-ray diffractometer with cobalt and copper generators), and desiccator were the equipment used in the study.

Methods

Synthesis of the metal-organic framework

Synthesis of MIL-100 (Fe) (Lavazza Institute)

Two primary solutions were used for the synthesis: a) a solution with pH = 11, containing 1.676 g (7.6 mM) trimesic acid dissolved in 23.72 g, NaOH 1 M (22.8 mM), and b) a solution with pH =2.7, prepared by dissolving 2.26 g (11.4 mM) of $FeCl_24H_2O$ in 97.2 g of water (Figure 2). The first solution was added dropwise to the second one while stirring, and a mixture with a molar ratio of Fe 1.5/H_2 O880/NaOH 3/H_3BTC 1 was synthesized (pH = 5.2). Stirring at room temperature was continued for 24 hours. The formed crystalline precipitates were separated by centrifugation at 3700 rpm, followed by washing in triplicates with water and once with ethanol. The specimen was dried at room temperature, and accordingly, 4.01 g of MIL-100 (Fe) powder with 76% efficiency was produced [9].

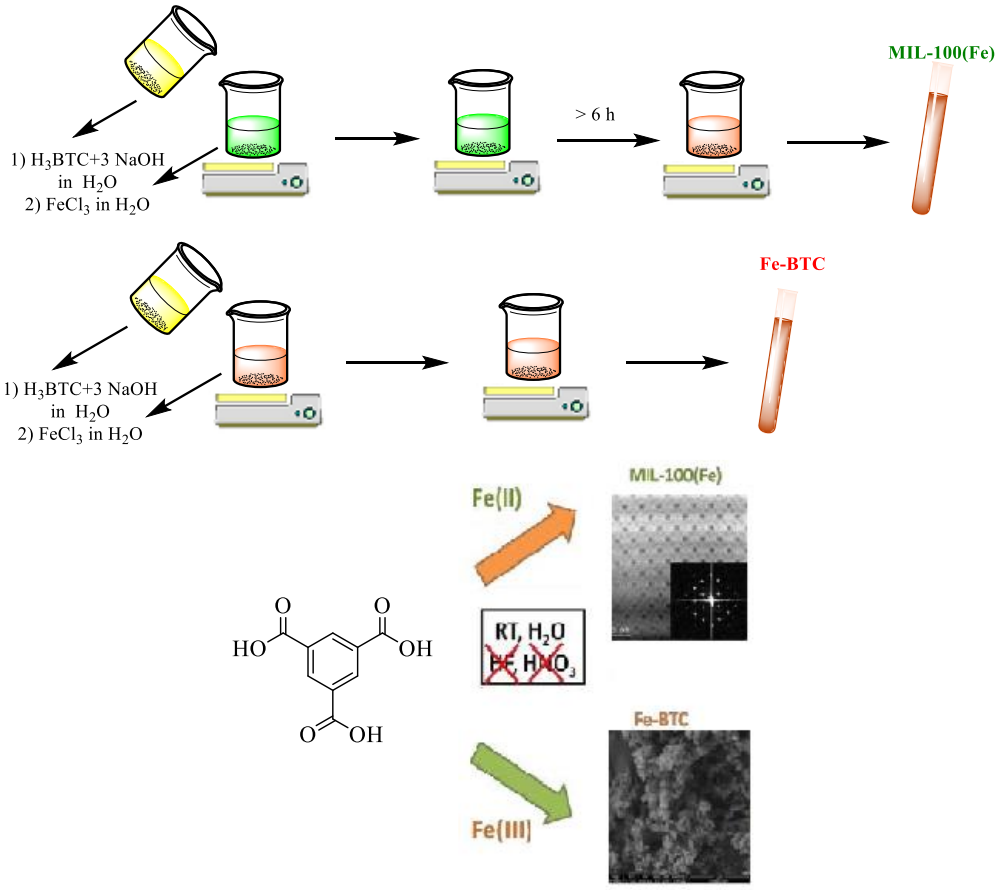

Figure 2: (Up) synthesis of MIL-100(Fe) and Fe-BTC [14]; (down) synthesis and the three-dimensional structure of MIL-100(Fe)

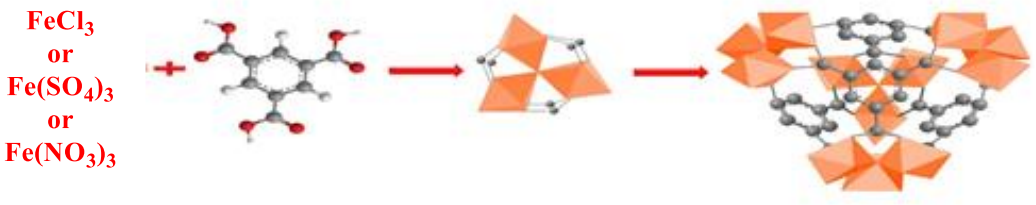

Figure 3: MIL-100 (Fe) structure by scanning tunneling electron microscope; a) at magnification <650 µm; b) corners; c) crystal pores resolution [14]

Synthesis of Fe-BTC

The semi-amorphous Fe-BTC is prepared similar to Basolite 300F, a commercial material. It was synthesized using two solutions: a) a colorless solution with pH ~ 11 that was prepared by dissolving 0.263 g of trimesic acid in 10/150 g of an aqueous solution sodium hydroxide (1M) and b) a yellowish-orange solution with pH 1.8 prepared by dissolving 0.508 g of $FeCl_3(H_2O)_6$ in 10 g of water; then the second solution was added dropwise, under a magnetic stirrer, to the first one (Figure 2). A solid brown-orange precipitate of Fe-BTC was produced. The suspension (pH ~ 1.2) was left for 10 minutes under the stirrer at room temperature (23 °C). The molar composition of the final mixture was exactly similar to that of MIL-100 (Fe) (1.5 Fe, $1H_3BTC$, 3NaOH, 880 H_2O). The brown precipitate was separated by centrifugation and then washed with deionized water and ethanol and left to dry at room temperature.

After the identification of features and characterization of structures, the synthesized compound was utilized for the removal of lead at different concentrations. The concentration of lead was measured at 520 nm after and before the adsorption process by an atomic absorption spectrometer. The adsorbent value was within the range of 0.2-0.5 mg/L; the lead concentration was 50-150 mg/L, the temperature was 10-75 °C, and the pH was 3.5-12.5 (Figure 3) [10].

Result and Dissection

The specific area and diameter of pores in the adsorbent were investigated. Considering many unsaturated surfaces and active sites in the adsorbent, the lead adsorption rate was high at the beginning of the adsorbent and the lead cation contact processes. There is a significant amount of hydronium ion in the environment. On the other hand, the surfaces of synthesized adsorbent have benzenetricarboxylate ligands with three negative charges and a high affinity to neutralize, which due to the acidity of the environment, neutralize negative charges on the adsorbents and make the adsorbent stable. Besides, due to the presence of an electron-donating group on the benzene ring in the adsorbent ligand and higher electronegativity of lead than iron, the lead metal was trapped (electronegativity of lead is higher than that of iron (2.33 vs. 1.83); therefore, the removal of lead was non-electrostatic. The adsorption of lead continued until saturation and then it was fixed, which was due to the full removal of lead ions from the solution. Therefore, the efficiency of the process was highly dependent on the lead concentration in the solution. Increased removal rate following the increase in adsorbent amount was due to more availability of surface areas on the adsorbent and more effective contacts between the vacant sites and lead cations in the aqueous solution; the removal rate even increases with increasing the active surface of the catalyst. The reason for this is the overlap of adsorption removal sites in the first phase, and then their synergy to make it stable in terms of the number of adsorption sites and adsorption rate.

Magnetization

The magnetization of the synthesized Fe-BTC metal-organic framework was calculated based on the Faraday law with a measurement range of zero Oe, using the Langevin equation (cm/g/s). According to Figure 4, the synthesized framework has magnetic properties, increasing with an increase in the magnetic field.

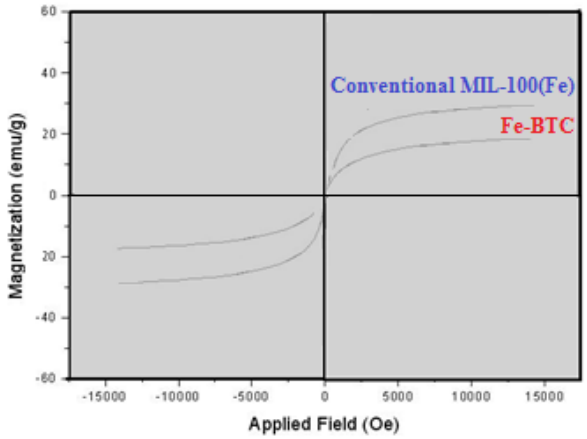

Figure 4: Hysteresis curve by Oe [16]

Langevin equation (1) is as follows:

$$D_m = \left(\frac{18K_BTx_{in}}{\pi\sigma_0\rho^2}\right)^{\frac{1}{3}} \quad (1)$$

Since the curve passed through the origin, coercivity field and magnetization hysteresis were not observed. So, the framework synthesized at room temperature was superparamagnetic particles (Table 1).

Table 1: Magnetic parameters of the framework

Framework	Temperature, °C	Magnetic density, ρ (g/cm^3)	The diameter of crystal particles, nm	Magnetic saturation, σS (emu/g)
MIL-100(Fe)	60	5.55	7.11	30
Fe-BTC	60	16.66	6.35	20

The lead absorption rate (mg/g) was calculated by equations (2) and (3), where Ce is the equilibrium and C0 the initial concentration of lead (ppm), M the result of dividing the weight of the adsorbent (g) by solution (L), and qe the absorption capacity (mg/g) [11].

Adsorption efficiency (2)

$$(R\%) = \frac{(C_0 - C_e) \times 100}{C_0}$$

The amount of lead absorbed (3)

$$(q_e) = \frac{(C_0 - C_e)}{M}$$

Intensive distribution of particle sizes

According to the results, the synthesized specimen was 30-36 nm on average (a 50 <d <2 nm mesoporous material) (Figure 5).

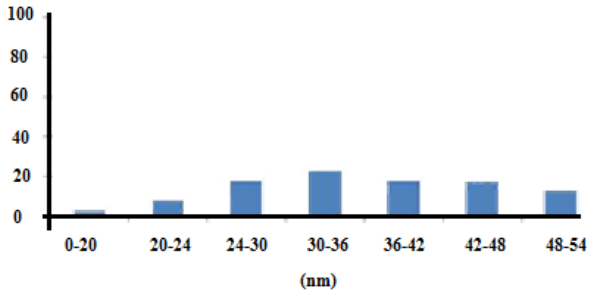

Figure 5: Intensive distribution of particle sizes

Scanning tunneling electron microscopy

This microscope is used for imaging the external surfaces, including the shape and size of particles. It was used for direct examination and measurement of crystals, and the results were consistent with those of an X-ray analyzer. The

images taken by this microscope showed that the synthesized Fe-BTC had a stable structure and consisted of amorphous quasi-cluster units in terms of internal morphology (Figure 7) [12].

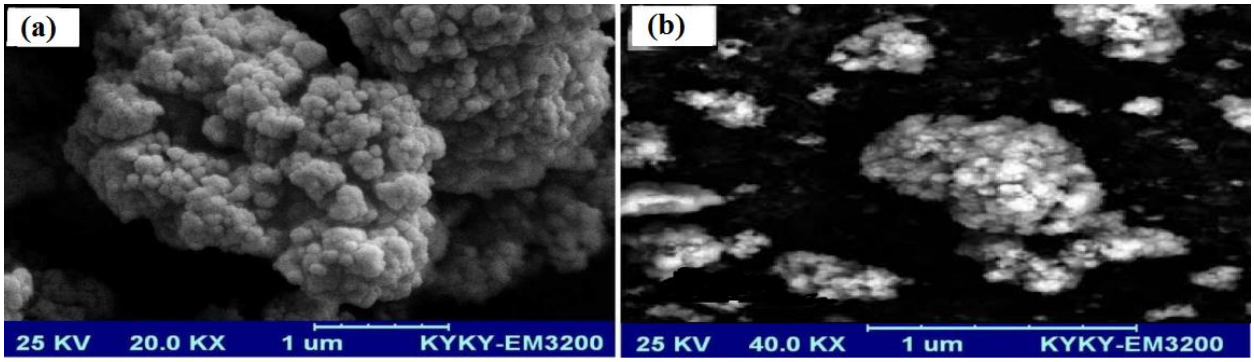

Figure 6: Scanning electron microscope Fe-BTC; a) scanning electron, b) scanning tunne

Gravimetry

In terms of thermogravimetric analysis, the structure of MIL-100 (Fe) was compared with that of the commercially available compound (Figure 7). Analysis of an organic ligand is a one-step process; an ignorable difference was observed between them that can be attributed to the uncontrolled atmosphere of synthesis and the presence of ions (fluoride) in the commercial framework, replaced by hydroxide at room temperature in the synthetized specimen. Two-stage analysis of Fe-BTC at 307 °C and weight loss was exclusively attributed to the decomposition of H_3BTC and the residual of Fe_2O_3. The second stage of weight loss was related to the destruction of structures and conversion to iron (II, III) oxide. Removal of the organic ligand of MIL-100 (Fe) and synthetic MIL-100 (Fe) were observed in synthetic Fe-BTC at 403, 383, and 346 °C. The weight loss to the residual weight ratio were 1.53 and 1.68 in MIL-100 (Fe) and synthetic MIL-100 (Fe), respectively; it was also 2.22 for synthetic Fe-BTC, which was due to the excess amount of ligand in the structure of Fe-BTC. The thermal and structural resistance of the synthesized material was compared with its commercial form, using the same method. Observations indicated the excellent thermal resistance of structures.

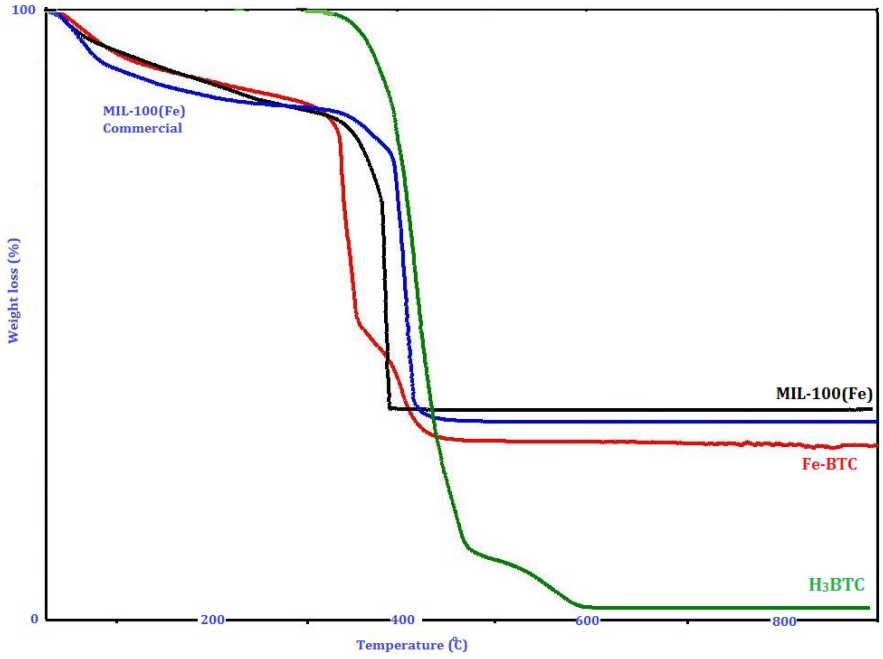

Figure 7: Thermogravimetric analysis by °C

X-ray diffraction

It is an old method to determine the qualitative properties, crystal orientation, etc., of compounds. The sharpness of the peaks indicates the purity, crystallinity, and single-phasic of the synthesized material. The average diameter of crystal particles is calculated by the information obtained by X-ray diffraction, such as the intensity and width of the peak. In Equation 4, D is the average particle size or diameter, K the Scherrer constant (0.9), X-ray wavelength (1.54060 Å), θ diffraction angle of each peak, and β the width of the peak at half the maximum height (°). Accordingly, wider peaks (such as iron oxides) are smaller in size, and their average size was 25 nm. The average diameter of crystal particles of Fe-BTC and MIL-100 (Fe) was 30 nm. Figure 8 illustrates the X-ray diffraction pattern at 50 °C and 120 th minute [13].

$$D=K\lambda/\beta \cos\theta \quad (4)$$

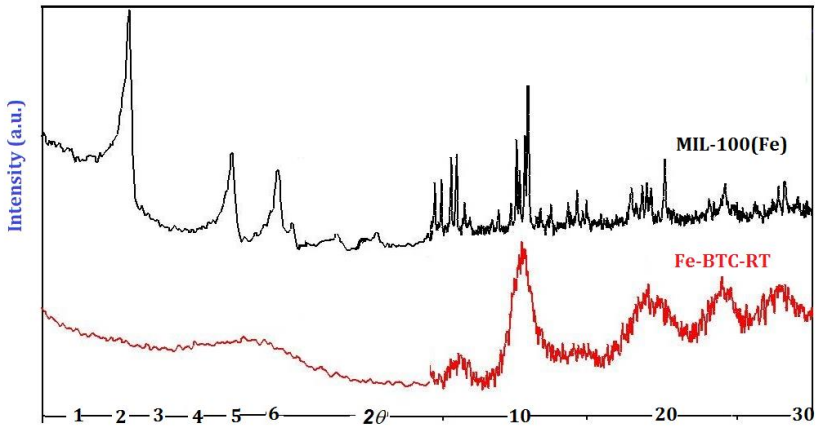

Figure 8: Comparison of X-ray diffraction patterns [17]

FTIR

It was used to confirm the functional group of synthetic structures, such as vibration peak OH (1449), CO (1383), benzene ring (759), etc. FTIR was used for the BTC framework with a vibration-tensile peak of Fe-O (484) (Figure 9) [14, 19].

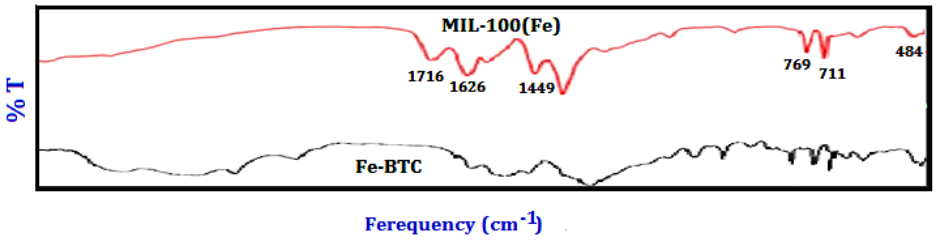

Figure 9: Comparison of FTIRs [15]

Functional groups of the structure by FTIR are shown in Table 2. A variety of benzenetricarboxylate resonant bonds were observed in Fe-BTC up to less than 1300 nm/cm, but in the range of 1300-1400, ligand bonds were observed with several sites on iron.

Table 2: Functional groups in FTIR

Framework	COOH	OH	C-O	OH	C-O	C-H	ArC-H	ArC-C	Fe-O
Feature		Tensile	Tensile	Vibration	Vibration-tensile of a benzene ring				
MIL-100-Fe	-	3414	1625	1449	1383	711, 759	-	-	484
Fe-BTC	-	-	-	-	-	-	3000	-	500

Ultraviolet-Vis

The structures of MIL-100 (Fe) and Fe-BTC were studied using the UV-Vis. With increasing irradiation time, the absorption rate decreased to the right side of the graph. The peak emerging at 344.5 nm is related to the ligand benzene ring (Figure 10) [14].

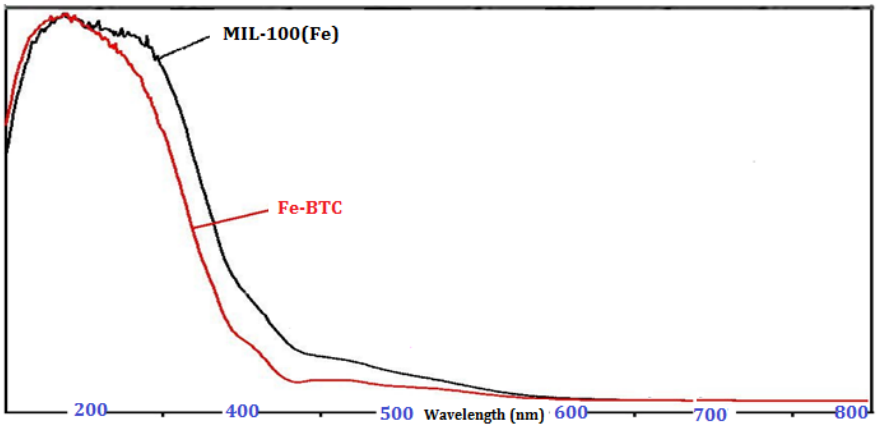

Figure 10: *Ultraviolet-Vis*

Effect of parameters

pH effect

The highest lead removal rate was observed under acidic conditions, and the maximum lead removal was in pH = 3.4. Given the solubility of lead hydroxide (10 E_20) multiplied by lead deposition gave a constant value under basic conditions. According to Daniel Denamur, it is unclear that the lead removal in pHs above 7 is related to adsorption or precipitation. Hence, neutral pH is considered optimal.

There was a pH range for each hydrolyzable metal ion, where the adsorption efficiency reaches its maximum (threshold of surface area adsorption). Due to the possible formation of lead hydroxide at higher pH values, the adsorption rate decreased [16].

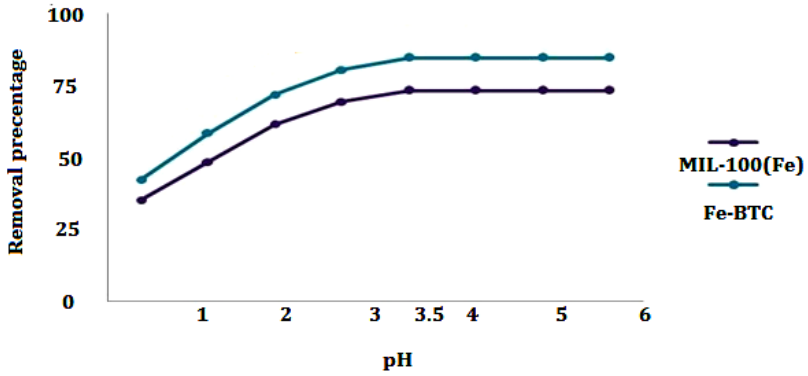

Figure 11: Effect of pH

Absorbent effect

To investigate the effect of adsorbent concentration, it was initially set at 0.10 mg/L. With increasing the adsorbent amount from 0.15 to 0.25 mg/L, the lead removal rate increased from 90% to 100% but did not change with a further increase of adsorbent (Figure 12).

As the adsorbent concentration increased, the number of free sites for adsorption increased until all the lead in the solution was absorbed by the active sites on the adsorbent surface.

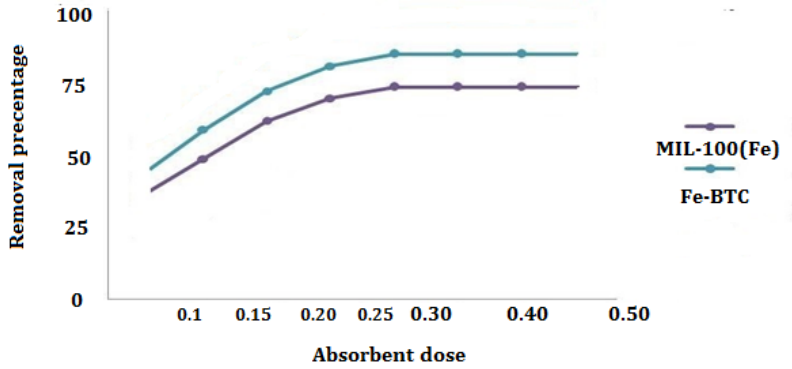

Figure 12: Effect of absorbent concentration (mg/L) on lead removal

Effect of lead concentration

Lead concentration was investigated within the range of 10-150 mg/L. 100% removal was obtained by keeping the amount of adsorbent constant at a minimum of 0.1 mg/L, and lead concentration at 10 mg/L. Nevertheless, with increasing lead concentration and keeping adsorbent constant at 0.1 mg/L, the removal efficiency decreased, which could be due to the occupation of all adsorbent sites and their vacancy at lower concentrations. Besides, 100% removal was obtained at adsorbent, and lead concentrations of 0.5 and 150 mg/L, respectively, and the efficiency remained unchanged with increasing the lead concentration (Figure 13).

It is associated with an increase in the adsorbent concentration, while the lead concentration is constant, and an increase in free surface sites, causing them to remain vacant. Therefore, the adsorption rate remained constant, and the adsorption capacity at equilibrium (Qe) decreased.

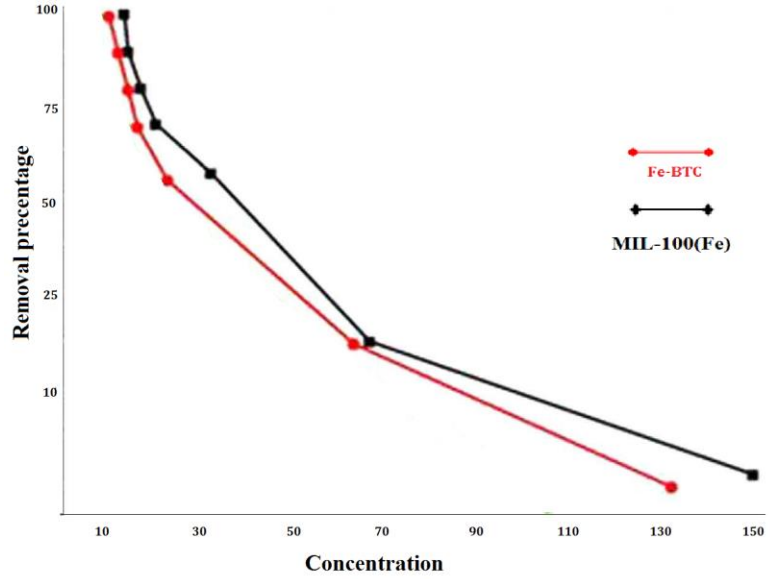

Figure 13 : Effect of lead concentration

Effect of temperature

The effect of temperature on lead removal was assessed within the range of 10-75 °C. The results showed that lead removal increased with increasing temperature, and the maximum removal was obtained at 50°C. Some water evaporated at 70-50°C, leading to volume

reduction, although the error was negligible (Figure 14).

With raising temperature, the adsorption rate increases while the higher temperature could reduce the adsorption rate, indicating physical adsorption.

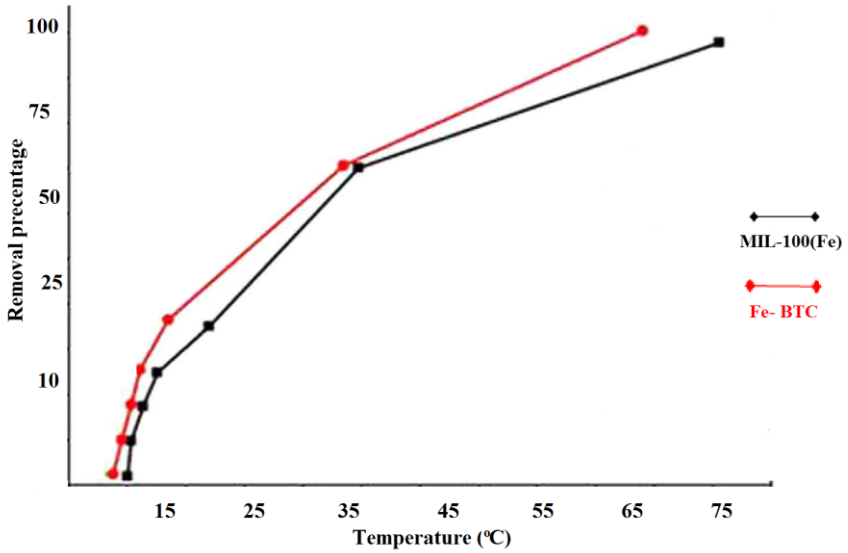

Figure 14: Effect of temperature (°C)

Absorption and absorption

The framework of the synthesized metal-organic adsorbent was separable after the adsorption of lead using an electric or magnetic field (1 Tesla in the present study), instead of applying a costly and difficult process of filtration. After washing the magnet containing metal-organic adsorbent with 5 mg/L of nitric acid (0.1-2 M) in five minutes and separation of lead, reduced frameworks could be reused in the system. The BTC-Fe framework could be reduced and reused in four repetitions.

Minitab software was used to design and evaluate four dependent variables at five levels, and the final output was calculated by Equation (5).

$$Y= \beta_0 + \sum \beta_j \cdot X_i + \sum \beta_{jj} \cdot X_j^{(2)} + \sum \beta_{jk} \cdot X_j \cdot X_k \quad (5)$$

where Y is efficiency, β_0 intersection point, β_j linear coefficient, β_{jj} squared coefficient, β_{jk} coefficient of interaction, and X_i, X_j^2, X_j, X_k the level of independent variables. As shown in Table 3, the number of specimens was estimated. The effect of adsorbent concentration on lead absorption is shown in Table 4.

Table 3: Range of variables

Variable			Surface		
	-α	-1	0	1	+α
pH	3.5	4	7	8	12.5
Lead concentration (mg/L)	10	75	100	120	150
Time, min	10	30	60	90	120
Adsorbent, mg/L	0.2	0.3	0.35	0.4	0.5

Table 4: Effect of adsorbent amount on lead removal rate

Initial lead concentration, ppm	Post-treatment lead concentration, ppm	Removed lead, mg/g	Adsorbent Amount, mg/L	Efficiency, %
150	33	117	0.15	78
150	15	135	0.20	90
150	0	150	0.25	100
150	0	150	0.35	100

Isothermal and kinetics

Absorption and desorption isotherm

To quantitatively and qualitatively determine the adsorption capacity, data is analyzed by isotherms. The two-parameter isotherm models of Langmuir and Freundlich are the most widely used ones (Equations 6 and 7).

Langmuir Equation (6)

$$\frac{c_e}{q_e} = \frac{c_e}{Q_0} + \frac{1}{Q_0^b}$$

Freundlich Equation (7)

$\ln q_e = \ln k + 1/n \ln c_e$

The experiment was performed with lead concentrations of 25, 40, 50, 75, and 150 mg/L, acidic pH, stirrer speed of 150 rpm, temperatures of 30, 40, and 50°C, nanoparticles concentration of 0.25 mg/L, and recirculation within two hours, and then the results were compared with Langmuir, Freundlich, and BET models. The adsorption and desorption curve, based on IUPAC classification, was type IV, which had a drastic increase in adsorption at the relevant pressure of less than 0.1, and a hysteresis curve at a high relative pressure of 0.1-1.7, indicating the presence of mesoporous and microporous materials. The absorption of lead in BTC-Fe followed the Langmuir model, physical adsorption. Figure 15 shows the adsorption isotherm; BTC-Fe pores had only one space of 25 Å and a window of 4.8 x 5.8 Å in diameter.

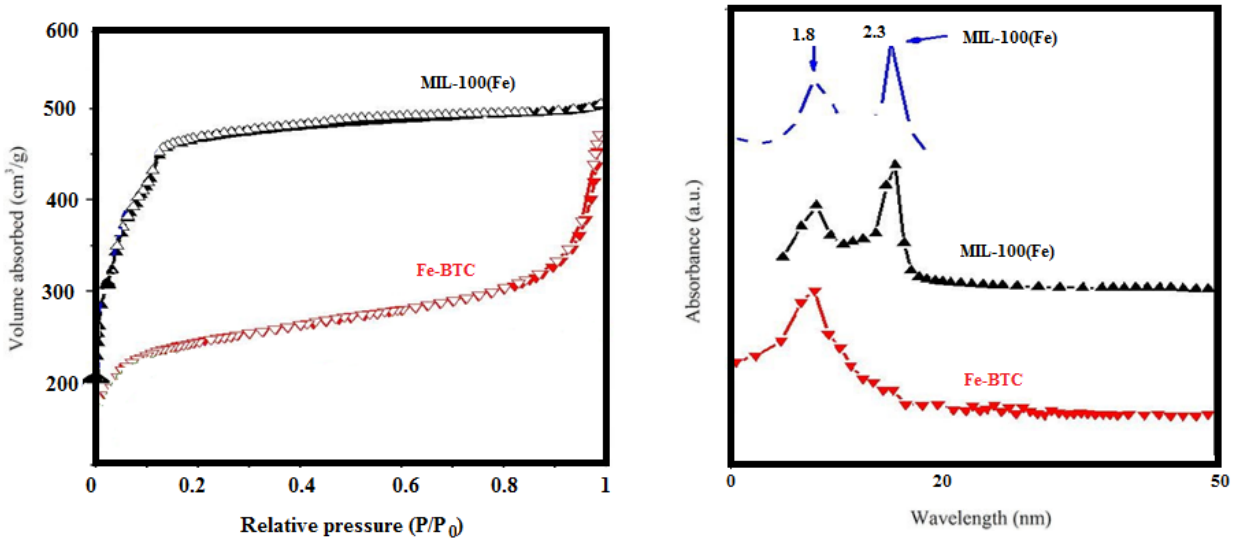

Figure 15: (Left) isotherms of absorption (filled) an desorption (empty) (right) [12]

Kinetics of adsorption reactions

To investigate the mechanism of adsorption and control of the rate of reaction stages, such as progress and mass transfer, kinetic models with first and second-order equations were used, and the rate of lead removal was investigated in terms of pseudo-first- and second-order reactions (Equations 8 and 9). The results are

shown in Table 5, and the Fe-BTC adsorption process followed a pseudo-second-order kinetic model.

Table 5: Absorption parameter in Fe-BTC [15]

Temperature, °C 323 Fe-BTC	Parameter Isotherm Langmuir
925	Q_{max}, mg/g
0.014	b/ L, mg
0.995	R^2
2.7×10^4	Kd, mg/g
Fe-BTC	Freundlich
12.181	K, mg/g
0.4	1/n, mg
0.933	R^2

$$\frac{t}{q_t} = \frac{1}{k_2 q_e^2} + \frac{t}{q_e} \quad (8)$$

$$K_d = \frac{C_i - C_f}{C_f} \times \frac{V}{m} \quad (9)$$

BJH analysis

The results of BJH analysis, including the distribution curve of pore sizes and the nitrogen adsorption and desorption isotherms, are shown in Table 6. The hysteresis curve at relatively high pressures illustrates high porosity and surface area in the synthesized framework [14].

Table 6: Physicochemical properties of the adsorbent [18]

Metal-organic specimen Synthetized at room temp.	Pore diameter, nm Peak of PSD	The specific volume of the pore (cm^3/g) $p/p_0 = 0.98$	The total specific surface area of BET, m^2/g $total_{SBET}$ – $S_{BETmicroporosity}$	Langmuir specific surface area, m^2/g	The specific surface area of BET, m^2/g
Fe-BTC at room temp.	925-950.3	900	204	0.65	1.85
MIL-100-1	855	910	72	0.4	1.81

Table 7: Parameters of reaction rate [14]

Adsorbent	First-order reaction			Second-order reaction		
	K1	Qe	R^2	K2	Qe	R^2
	Slope, min	mg/g		y-intercept, g/mg/min	mg/g	
Fe-BTC	0.025	32.237	0.97	0.880	40.013	0.99

Conclusion

In the present study, Iron–benzenetricarboxylate metal-organic frameworks were prepared and then was identified and characterized by many techniques. The results of the present study are in agreement with those of the study by Alizadeh et al. (2011), on lead removal with magnetic iron nanoparticles, reporting the efficiency of 70% in pH 4, and also the lead removal by 2-mercaptobenzothiazole functionalized magnetic Fe. The high correlation between lead removal and its initial concentration in solution is related to the number of active sites on the adsorbent surface. As the concentration of lead increases, the removal rate also increases in the solution; however, despite an increase in lead concentration, some sites are still available for binding, which as a result, improve the efficiency of the process. Magnetic iron and iron oxide nanostructures modified with BTC ligand, due to high surface area, separability, and recyclability, significantly reduce the cost of preparation (Fe-BTC adsorbent can be used in four repetitions without losing the capacity), and hence are more suitable than other magnetic nanoparticles and methods to remove lead from effluents, adsorb with maximum power and energy, prevent the entry of nanomaterials into the environment, and also prevent waste generation.

Funding

This research did not receive any specific grant from funding agencies in the public, commercial, or not-for-profit sectors.

Authors' contributions

All authors contributed toward data analysis, drafting and revising the paper and agreed to be responsible for all the aspects of this work.

Conflict of Interest

We have no conflicts of interest to disclose.

References

[1]. Alkherraz A., Ali A., Elsherif K., *J. Med. Chem. Sci.,* 2020, **3**:1 [Crossref], [Google Scholar], [Publisher]

[2]. Shahbazi A., Younesi H., Badiei A., *J. Water Wastewater,* 2012, **23**:13 [PDF], [Google Scholar], [Publisher]

[3]. Alizadeh R., Abedini S., Bidhendi N., Amoabediny G., *Iran. Institute Res. Dev. Chem. Indust.,* 2011, **30**:71 [PDF], [Google Scholar], [Publisher]

[4]. B. Baghernejad, M. Fiuzat, *J. Appl. Organomet. Chem.,* 2021, **1**:17 [Crossref], [Google Scholar], [Publisher]

[5]. Mahdavi M., Ahmad M.B., Haron M.J., Gharayebi Y., Shameli K., Nadi B., *J. Inorg. Organomet. Polym.,* 2013, **23**:599 [Crossref], [Google Scholar], [Publisher]

[6]. Eddaoudi M., Moler D.B., Li H., Chen B., Reineke T.M., O'keeffe M., Yaghi O.M., *Acc. Chem. Res.*, 2001, **34**:319 [Crossref], [Google Scholar], [Publisher]

[7]. X. Liu, Y. Zhou, J. Zhang, T. Lin, L. Lin, G. Zeng, *ACS App. Mater. Interfaces.*, 2017, **20**:800 [Crossref], [Google Scholar], [Publisher]

[8]. M. Feng, P. Zhang, H.C. Zhou, V.K. Sharma, Chemosphere, 2018, **209**:783 [Crossref], [Google Scholar], [Publisher]

[9]. M. Cheng, C. Lai, Y. Liu, G. Zeng, D. Huang, C. Zhang, L. Qin, L. Hu, C. Zhou, W. Xiong, *Coord. Chem. Rev.,* 2018, **368**:80 [Crossref], [Google Scholar], [Publisher]

[10]. K. Cui, B. Yan, Y. Xie, H. Qian, X. Wang, Q. Huang, Y. He, S. Jin, H. Zeng, *J. Hazard Mater.,* 2018, **350**:66 [Crossref], [Google Scholar], [Publisher]

[11]. M. Hossein Zadeh, N. Keramati, M. Mehdipour Ghazi, *J. Iran. Chem. Soc.,* 2019, **16:**401 [Crossref], [Google Scholar], [Publisher]

[12]. X. Zhao, S. Liu, Z. Tang, H. Niu, Y. Cai, W. Meng, F. C. Wu, J. P. Giesy, *Sci. Rep.,* 2015, **5**:11849 [Crossref], [Google Scholar], [Publisher]

[13]. F. Ke, J. Jiang, Y. Li., J. Liang, X. Wan, S. Ko, *Appl. Surf. Sci.*, 2017, **413**:266 [Crossref], [Google Scholar], [Publisher]

[14]. K. Guesh, C.A.D. Caiuby, A. Mayoral, M. Díaz-García, I. Díaz, M. Sanchez-Sanchez, *Cryst. Growth Des.,* 2017, **17**:1806 [Crossref], [Google Scholar], [Publisher]

[15]. N.M. Mahmoodi, J. Abdi, M. Oveisi, M.A. Asli, M. Vossoughi, *Mater. Res. Bull.*, 2018, **100**:357 [Crossref], [Google Scholar], [Publisher]
[16]. K. Petcharoen, A. Sirivat, *Mater. Sci. Eng., B,* 2008, **177**:421 [Crossref], [Google Scholar], [Publisher]
[17]. M. Du, L. Li, M. Li, R. Si, *RSC Adv.,* **2016**, *6*, 62705 [Crossref], [Google Scholar], [Publisher]
[18]. H. Jiangbo, C. Haojie, F. Minglai, Y. Baoling, *Sci. Sin. Chim.,* 2017, **47**:830 [Crossref], [Google Scholar], [Publisher]
[19]. F. Ke, L.G. Qiu, Y.P. Yuan, X. Jiang, J.F. Zhu, *J. Mater. Chem*., 2012, **22**:9497 [Crossref], [Google Scholar], [Publisher]

HOW TO CITE THIS ARTICLE
Gholamreza Nabi bidhendi, Naser Mehrdadi, Mehran Firouzbakhsh. Removal of Lead from Wastewater by Iron–Benzenetricarboxylate Metal-Organic Frameworks, Chem. Methodol., 2021, 5(3) 271-284
DOI: 10.22034/chemm.2021.130208
URL: http://www.chemmethod.com/article_130208.html